

Robust Unsupervised Domain Adaptation for Neural Networks via Moment Alignment

Werner Zellinger, Bernhard A. Moser, Thomas Grubinger, Edwin Lughofer,
Thomas Natschlager, and Susanne Saminger-Platz

Abstract—A novel approach for unsupervised domain adaptation for neural networks is proposed that relies on a metric-based regularization of the learning process. The metric-based regularization aims at domain-invariant latent feature representations by means of maximizing the similarity between domain-specific activation distributions. The proposed metric results from modifying an integral probability metric in a way such that it becomes translation-invariant on a polynomial reproducing kernel Hilbert space. The metric has an intuitive interpretation in the dual space as sum of differences of central moments of the corresponding activation distributions. As demonstrated by an analysis on standard benchmark datasets for sentiment analysis and object recognition the outlined approach shows more robustness w.r.t. parameter changes than state-of-the-art approaches while achieving even higher classification accuracies.

Index Terms—transfer learning, domain adaptation, neural networks, moment alignment, integral probability metric

I. INTRODUCTION

THE problem of training a machine learning model in the presence of different training and test distributions is known as *domain adaptation* [3], [6]–[9]. The goal of domain adaptation is to build a model that performs well on a *target* distribution while it is trained on a different but related *source* distribution.

One important example is in the sentiment analysis of product reviews [1], where a model is trained on data of a source product category, e.g. kitchen appliances, and it is tested on data of a related category, e.g. books. A second example is the training of image classifiers on unlabeled real images by means of nearly-synthetic images that are fully labeled but which have a distribution that is different [2], [3]. Another example is the content-based depth range adaptation of unlabeled stereoscopic videos by means of labeled data from movies [4], [5].

It is shown in [10], that a classifier’s error on the target domain can be bounded in terms of its error on the source domain and a difference between the source and the target domain distribution [10]. This motivated many approaches to first extract features that overcome the distribution difference and subsequently minimize the source error [8], [11]–[13]. With the recent developments in representation learning, approaches have been developed that embed domain adaptation in the feature learning process. One way for doing so is by

minimizing a combined objective that ensures both, a small source error and feature representations that overcome the domain difference [3], [14], [15].

While much research has been devoted to the question of how to supervised minimize the source error [16], [17], relatively little is known about objectives that ensure domain-invariant feature representations. In this contribution we focus on the latter question. In particular, we deal with the task of *unsupervised domain adaptation* where no information about the target labels is available. However, the proposed approach is also applicable under the presence of target labels (*semi-supervised domain adaptation*).

We aim for a robust objective function. That is, (a) the convergence of our learning algorithm to sub-optimal solutions should guarantee similar domain-specific activation distributions and (b) the accuracy of our learning algorithm should be insensitive to changes of the hyper-parameters. The latter property is especially important in the unsupervised problem setting since the parameters have to be selected without label information in the target domain and the application of parameter selection routines for hierarchical representation learning models can be computationally expensive.

One simple idea to approach both properties is to minimize an integral probability metric [18] between the domain-specific hidden activation distributions that is based on a polynomial function space [19]–[22]. However, it can be shown that instability issues arise when higher order polynomials are considered. We solve these issues by modifying an integral probability metric in a way such that it becomes translation-invariant on a polynomial reproducing kernel Hilbert space. We call the metric the Central Moment Discrepancy (CMD). The CMD has an intuitive representation in the dual space as sum of differences of central moments of the corresponding distributions.

We propose a robust domain adaptation algorithm for the training of neural networks that is based on the minimization of the CMD. The classification performance and accuracy sensitivity w.r.t. parameter changes is analysed on artificial data as well as on benchmark datasets for sentiment analysis of product reviews [12] and object recognition [23].

The main contributions of this work are as follows.

- We propose a novel approach for unsupervised domain adaptation for neural networks that is based on a metric-based regularization of the learning process. We call the metric the Central Moment Discrepancy (CMD).
- We prove several appealing properties of the CMD including its computationally efficiently implementable

This work has been partly funded by the Austrian COMET Center SCCH. We thank Florian Sobieczky for helpful discussions. The source code of the experiments is publicly available (<https://github.com/wzell/mann>).

dual representation, a relation to weak convergence of distributions and a strictly decreasing upper bound for its moment terms.

- Our algorithm outperforms comparable approaches on most domain adaptation tasks on two standard benchmark datasets for sentiment analysis of product reviews and object recognition.

In addition, our approach is robust w. r. t. the following aspects.

- Our approach overcomes instability issues of the learning process by solving the problem of mean over-penalization that arise in the application of integral probability metrics based on polynomial function spaces.
- Our algorithm can be used with a fixed weighting parameter for the domain adaptation regularization. In contrast to state-of-the-art approaches, our results on the object recognition dataset are obtained without data augmentation and without tuning of the learning rate.
- A post-hoc parameter sensitivity analysis shows that the classification accuracy of our approach is not sensitive to changes of the number of moments parameter and changes of the number of hidden nodes.

In Section II we give a brief overview of related work. In Section III we specify our model of domain adaptation and motivate the training of neural networks based on a joint objective that minimizes the source error and at the same time enforces similar hidden activation distributions. Section IV presents the idea of applying the integral probability metric based on a polynomial function space and discusses the problem of mean over-penalization. In Section V we propose the CMD and in Section VI we analyse some convergence properties. A gradient based algorithm for domain adaptation that minimizes the CMD is presented in Section VII. Section VIII analyses the classification performance and the parameter sensitivity of our algorithm based on benchmark datasets. Section IX concludes the work.

II. RELATED WORK

The problem of domain adaptation has been tackled by many approaches. In [6], [24]–[26] the emphasis is set on the analysis of linear hypothesis whereas more recently also non-linear representations have been studied including neural networks [1], [3], [14], [15], [27]–[29]. In the latter case, the source and the target domain distributions are aligned in the latent activation space in order to guarantee domain-invariant feature representations. Three prominent research directions can be identified for the choice of the alignment objective.

The first research direction investigates the re-weighting of the neural network activations such that specific mean and covariance features are aligned. These approaches work particularly well in the area of object recognition [30] and text classification [31]. Mean and covariance feature alignment has been extended to the minimization of the Frobenius norm between the covariance matrices of the neural network activations [15]. This distance function is parameter-free and it does not require additional unsupervised validation procedures or parameter heuristics. We show that these approaches can be further improved in terms of time complexity and prediction

accuracy by additionally considering moment characteristics of higher orders.

Another research direction investigates the minimization of the *Proxy-A distance* [10] for distribution alignment. This distance function is theoretically motivated and can be implemented by means of an additional classifier with the objective of separating the distributions. For distribution alignment, the gradient of the classifier is reversed during back-propagation [3]. Unfortunately, an additional classifier has to be trained in this approach including the need of new parameters, additional computation times and validation procedures. In addition, the reversal of the gradient causes several theoretical problems [32] that contribute to instability and saturation during training. Our approach achieves higher classification accuracies on several domain adaptation tasks on benchmark datasets.

A third research direction applies a distance function called Maximum Mean Discrepancy (MMD) [33]. It is an integral probability metric that is based on the unit ball of a reproducing kernel Hilbert space (RKHS). Different underlying kernel functions lead to different RKHSs and therefore to different versions of the MMD. There exist approaches that are based on linear kernels [34], [35] which can be interpreted as mean feature matching. In [14] a combination of Gaussian kernels is used. They tackle the sensitivity of the MMD w. r. t. changes of the Gaussian kernel parameter by means of a combination of different kernels with heuristically selected parameters. In addition, the approach comes with the theoretical knowledge from the studies about RKHSs [36] and a linear-time implementation. Unfortunately, the tuning of the Gaussian kernel parameter is sophisticated in our unsupervised problem setting. We solve this issue by proposing a distance function that is less sensitive to changes of its parameter. Consequently, we obtain higher classification accuracies, than comparable approaches that are based on the Gaussian kernel, on two benchmark datasets.

Recently, some approaches focus on combining research about specific neural network architectures with the application of the MMD with Gaussian kernel [28], [29], [37]. Our approach is not restricted on multiple layers or network architectures. Actually, it can be combined with these ideas.

A part of this paper has been published as a conference paper [38]. This version considerably extends the conference publication by a target error bound based on integral probability metrics (Section III-A and Appendix-A), a mathematical motivation for applying distribution alignment on hidden activation distributions (Section III-B), the introduction of a polynomial RKHS (Section IV and Appendix-B), the description of the mean over-penalization problem (Section IV-A), the analysis of some theoretical properties of the CMD (Section VI, Appendix-D and Appendix-E), the experiments on an artificial dataset (Section VIII-B), additional implementations of related approaches (Section VIII-C) and the evaluations of the proposed algorithm based on the pre-trained model of [39] with different optimization strategies on the object recognition dataset (Section VIII-D).

III. PROBLEM DESCRIPTION OF DOMAIN ADAPTATION

Without loss of generality let us formulate the problem of unsupervised domain adaptation for binary classification [3], [10]. We define a *domain* as a pair of a distribution \mathcal{D} on inputs \mathcal{X} and a labeling function $g : \mathcal{X} \rightarrow [0, 1]$, which can have a fractional value when labeling occurs non-deterministically. We denote $\langle \mathcal{D}_S, g_S \rangle$ the *source* domain and $\langle \mathcal{D}_T, g_T \rangle$ the *target* domain. In order to measure to which extent a classifier $h : \mathcal{X} \rightarrow [0, 1]$ disagrees with a given labeling function g the expectation of its difference w.r.t. to the distribution \mathcal{D}_A is considered

$$\epsilon_A(h, g) = \mathbb{E}_{\mathcal{D}_A} [|h - g|].$$

We refer to $\epsilon_S(h, g_S)$ as the source error and to $\epsilon_T(h, g_T)$ as the target error.

In our problem setting, two samples are given: a labeled source sample $S = \{(\mathbf{x}_i, g_S(\mathbf{x}_i))\}_{i=1}^m \subset \mathcal{X} \times [0, 1]$ and an unlabeled target sample $T = \{\mathbf{x}_j\}_{j=1}^n \subset \mathcal{X}$. The goal of unsupervised domain adaptation is to build a classifier $h : \mathcal{X} \rightarrow [0, 1]$ with a low target error $\epsilon_T(h, g_T)$ while no information about labels in the target domain is given.

A. Motivation for Unsupervised Domain Adaptation

To motivate the problem of unsupervised domain adaptation let us first show how the error minimization in the target domain relates to the minimization of the source error and the difference between the domains $\langle \mathcal{D}_S, g_S \rangle$ and $\langle \mathcal{D}_T, g_T \rangle$.

In practice, we expect the difference between the labeling functions g_S and g_T to be small [10] or even zero [40]. Otherwise, there is no way to infer a good estimator based on the training sample [41]. Therefore, we focus on the distance between the distributions \mathcal{D}_S and \mathcal{D}_T . A suitable class of distance measures are integral probability metrics [18]. Given a function class $\mathcal{F} = \{f : \mathcal{X} \rightarrow \mathbb{R}\}$, an integral probability metric is defined by

$$d_{\mathcal{F}}(\mathcal{D}_S, \mathcal{D}_T) = \sup_{f \in \mathcal{F}} |\mathbb{E}_{\mathcal{D}_S}[f] - \mathbb{E}_{\mathcal{D}_T}[f]|. \quad (1)$$

Integral probability metrics play an important role in probability theory [42] and statistics [19]. According to [18] an integral probability metric is a pseudo-metric and it is a metric if and only if the function class \mathcal{F} separates the set of all signed measures μ with $\mu(\mathcal{X}) = 0$ [18, page 432].

Based on these results we may determine a first bound on the classifier's target error (see Appendix-A for its proof).

Theorem 1 (Target error bound): Let $h : \mathcal{X} \rightarrow [0, 1]$ be a classifier, then

$$\epsilon_T(h, g_T) \leq \epsilon_S(h, g_S) + d_{\mathcal{F}}(\mathcal{D}_S, \mathcal{D}_T) + \min \{ \mathbb{E}_{\mathcal{D}_S} [|g_S - g_T|], \mathbb{E}_{\mathcal{D}_T} [|g_S - g_T|] \} \quad (2)$$

with a suitable function class \mathcal{F} that contains $|h - g_S|$ and $|h - g_T|$.

Under the assumption on the difference between g_S and g_T to be small, Theorem 1 shows that the source error is a good indicator for the target error if the two domain distributions \mathcal{D}_S and \mathcal{D}_T are similar with respect to an integral probability metric defined in Eq. (1).

B. Domain Adaptation with Neural Networks

As example let us consider a continuous model of a neural network classifier $h = h_1 \circ h_0$ consisting of a representation learning part $h_0 : \mathcal{X} \rightarrow \mathcal{A}$ from the inputs $\mathcal{X} \subset \mathbb{R}^m$ to the activations $\mathcal{A} \subset \mathbb{R}^m$ and a classification part $h_1 : \mathcal{A} \rightarrow [0, 1]$ from the activations to the labels $[0, 1]$. Assume h_0 to be an invertible function from \mathcal{X} to \mathcal{A} . Then, for each continuous function p and distribution \mathcal{D} , the “change of variables” theorem [43, Theorem 9.8.2] yields

$$\int_{\mathcal{X}} p \circ h_0 d\mathcal{D} = \int_{\mathcal{A}} p d(h_0 \circ \mathcal{D}),$$

which implies that

$$d_{\mathcal{F}}(\mathcal{D}_S, \mathcal{D}_T) = d_{\mathcal{P}}(h_0 \circ \mathcal{D}_S, h_0 \circ \mathcal{D}_T), \quad (3)$$

where $\mathcal{P} = \{h_0 \circ f | f \in \mathcal{F}\}$.

Eq. (3) allows to minimize $\epsilon_T(h, g_T)$ in Eq. (2) by aligning the distribution of the activations $h_0 \circ \mathcal{D}_S$ and $h_0 \circ \mathcal{D}_T$ rather than the domain distributions \mathcal{D}_S and \mathcal{D}_T . In addition, Eq. (3) allows to focus on simple function classes \mathcal{P} , e.g. polynomials, that are suitable for the alignment of neural networks activation distributions $h_0 \circ \mathcal{D}_S$ and $h_0 \circ \mathcal{D}_T$ rather than considering complex function classes \mathcal{F} that are suitable for general domain distributions \mathcal{D}_S and \mathcal{D}_T .

A realization of this idea based on gradient descent is shown in Fig. 1.

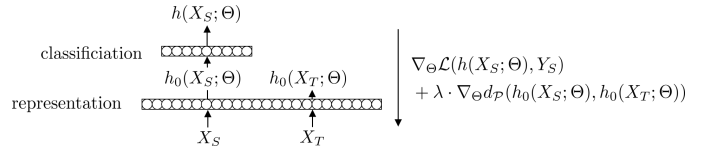


Fig. 1: Schematic sketch of a feed-forward neural network $h(X; \Theta)$ with parameters Θ optimized via gradient descent based on the minimization of a source loss $\mathcal{L}(h(X_S; \Theta), Y_S)$ and the minimization of a distance $d_{\mathcal{P}}$ between the activations $h_0(X_S; \Theta)$ and $h_0(X_T; \Theta)$ of the source sample X_S and the target sample X_T , where Y_S denotes the labels in the source domain. The minimization of $d_{\mathcal{P}}$ ensures domain-invariant representations. ∇_{Θ} refers to the gradient w.r.t. Θ .

IV. INTEGRAL PROBABILITY METRIC ON A POLYNOMIAL FUNCTION SPACE

The question is which function set \mathcal{F} is suitable for the integral probability metrics in Eq. (1) used for aligning activation distributions. Distance measures that can be obtained by different function sets include the Wasserstein distance, the total variation distance and the Kolmogorov distance [19].

We concentrate on polynomial function spaces. Every analytic function is given as a sum of homogeneous polynomials, i.e. its power series. The application of truncated series of homogeneous polynomials are standardly used in approximation theory [44] and numerical analysis [45]. The expectations of polynomials are sums of moments. This allows a natural interpretation of how the function set \mathcal{F} in Eq. (1) acts on the activation distributions. In applications like image retrieval,

moments are known as robust distribution descriptors [46], [47].

Let us consider the vector-valued index $\iota = (\iota_1, \dots, \iota_k)$, where $\iota_j \in \{1, \dots, m\}$. We denote by $\nu^{(k)}$ the resulting m^k -tuple of monomials of degree k with m variables, i.e.

$$\nu^{(k)}(\mathbf{x}) := (\nu_\iota(\mathbf{x}))_\iota \quad (4)$$

where $\nu_\iota(\mathbf{x}) = \prod_{j=1}^k x_{\iota_j}$ for $\mathbf{x} \in \mathbb{R}^m$. Further, let us denote by \mathcal{P}^k the class of homogeneous polynomials $p : \mathcal{X} \rightarrow \mathbb{R}$,

$$\begin{aligned} p(\mathbf{x}) &= \langle \mathbf{w}, \nu^{(k)}(\mathbf{x}) \rangle \\ &= \sum_{\iota} \omega_\iota \nu_\iota(\mathbf{x}) \end{aligned} \quad (5)$$

with $\|\omega\|_2 = \sqrt{\sum_{\iota} \omega_\iota^2} \leq 1$ for $\omega \in \mathbb{R}^m$. For example, the polynomials in \mathcal{P}^2 w.r.t. a distribution \mathcal{D} are corresponding linear combinations of the covariances of \mathcal{D} .

It is interesting to point out that this function space is closely linked to reproducing kernel Hilbert spaces [48]. Recall that a Hilbert space \mathcal{H} with inner product $\langle \cdot, \cdot \rangle_{\mathcal{H}}$ is a RKHS if and only if there is a positive definite kernel $\kappa : \mathcal{X} \times \mathcal{X} \rightarrow \mathbb{R}$ such that for all $f \in \mathcal{H}$ the reproducing property $f(x) = \langle f(\cdot), \kappa(x, \cdot) \rangle_{\mathcal{H}}$ is satisfied. κ is called the reproducing kernel of \mathcal{H} . The space of polynomials \mathcal{P}^k in Eq. (5) is the unit ball of a reproducing kernel Hilbert space $(\mathcal{H}, \langle \cdot, \cdot \rangle_{\mathcal{H}})$ with unique reproducing kernel

$$\kappa(\mathbf{x}, \mathbf{y}) := \langle \nu^{(k)}(\mathbf{x}), \nu^{(k)}(\mathbf{y}) \rangle_2. \quad (6)$$

This characterization of \mathcal{P}^k is proven in Appendix-B. Note that the integral probability metric with the function class being the unit ball of a RKHS is known as Maximum Mean Discrepancy [33].

A. The Problem of Mean Over-Penalization

Unfortunately, the MMD with the kernel in Eq. (6) and different other metrics [21], [22] suffer from the drawback of mean over-penalization which becomes worse with increasing polynomial order. For sake of illustration, let us consider two distributions \mathcal{D} and \mathcal{D}' on \mathbb{R} . For $k = 1$ we obtain

$$\begin{aligned} d_{\mathcal{P}^1}(\mathcal{D}, \mathcal{D}') &= \sup_{|f| \leq 1} |\mathbb{E}_{\mathcal{D}}[\omega x] - \mathbb{E}_{\mathcal{D}'}[\omega x]| \\ &= |\mu - \mu'|, \end{aligned} \quad (7)$$

where $\mu = \mathbb{E}_{\mathcal{D}}[x]$ and $\mu' = \mathbb{E}_{\mathcal{D}'}[x]$. Now, let us consider higher orders $k \in \mathbb{N}$. Assume the distributions \mathcal{D} and \mathcal{D}' have identical central moments $c_j(\mathcal{D}) := \mathbb{E}[(x - \mu)^j]$ but different means $\mu \neq \mu'$. By expressing the raw moment $\mathbb{E}_{\mathcal{D}}[x^k]$ by its central moments $c_j(\mathcal{D})$, we obtain, by means of the binomial theorem,

$$\begin{aligned} d_{\mathcal{P}^k}(\mathcal{D}, \mathcal{D}') &= |\mathbb{E}_{\mathcal{D}}[x^k] - \mathbb{E}_{\mathcal{D}'}[x^k]| \\ &= \left| \sum_{j=0}^k \binom{k}{j} c_j(\mathcal{D}) (\mu^{k-j} - \mu'^{k-j}) \right|. \end{aligned} \quad (8)$$

Since the mean values contribute in the sum of Eq. (8) by its powers, the metric in Eq. (1) with polynomials as function set is not translational invariant. Even, much worse, consider for

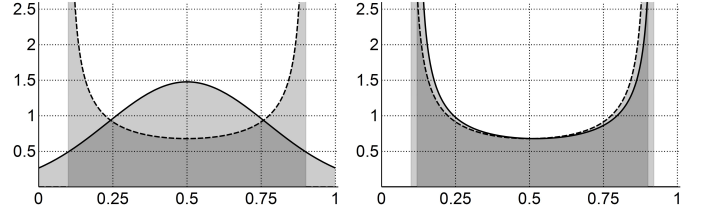


Fig. 2: Illustrative example of mean over-penalization problem. The MMD with standard polynomial kernel [33] and different other raw moment based metrics [21], [22] lead to counter-intuitive distance measurement as they consider the source Beta distribution (dashed) to be more similar to the Normal distribution on the left (solid) than to the slightly shifted Beta distribution on the right (solid).

example $\mu = 1 + \varepsilon/2$ and $\mu' = 1 - \varepsilon/2$, small changes of the mean values can lead to large deviations in the resulting metric, i.e. causing instability in the learning process.

For another example consider Fig. 2. Different raw moment based metrics consider the source Beta distribution (dashed) to be more similar to the Normal distribution on the left (solid) than to the slightly shifted Beta distribution on the right (solid). This is especially the case for the integral probability metrics in Eq. (1) with the polynomial spaces \mathcal{P}^1 , \mathcal{P}^2 and \mathcal{P}^4 , the MMD with the standard polynomial kernel $\kappa(x, y) := (1 + \langle x, y \rangle_2)^2$ and the cubic kernel $\kappa(x, y) := (1 + \langle x, y \rangle_2)^4$ [22], [33], and the integral probability metrics in [21]. See Appendix-C for the proof.

In the next section, we propose a metric that considers the right distributions as being more similar.

V. A PROBABILITY METRIC FOR DISTRIBUTION ALIGNMENT

Eq. (8) motivates us to look for a modified version of the integral probability metric that is translation-invariant. Therefore, we propose the following centralized version of the integral probability metric between the distributions \mathcal{D} and \mathcal{D}' :

$$\begin{aligned} d_{\mathcal{F}}^c(\mathcal{D}, \mathcal{D}') &:= \\ \sup_{f \in \mathcal{F}} |\mathbb{E}_{\mathcal{D}}[f(\mathbf{x} - \mathbb{E}_{\mathcal{D}}[\mathbf{x}])] - \mathbb{E}_{\mathcal{D}'}[f(\mathbf{x} - \mathbb{E}_{\mathcal{D}'}[\mathbf{x}])]|. \end{aligned} \quad (9)$$

We apply this modification on our problem of domain adaptation by introducing a “refined” metric as weighted sum of centralized integral probability metrics in Eq. (9) with unit balls of polynomial reproducing kernel Hilbert spaces of different orders

$$\text{cmd}_k(\mathcal{D}, \mathcal{D}') := a_1 d_{\mathcal{P}^1}(\mathcal{D}, \mathcal{D}') + \sum_{j=2}^k a_j d_{\mathcal{P}^j}^c(\mathcal{D}, \mathcal{D}'), \quad (10)$$

where $a_j \geq 0$, $d_{\mathcal{P}}$ and $d_{\mathcal{P}}^c$ are defined as in Eq. (1) and Eq. (9) w.r.t. the polynomial spaces \mathcal{P}^k , respectively. Note that in Eq. (10) for $k = 1$ we take $d_{\mathcal{P}^1}(\mathcal{D}, \mathcal{D}') = |\mu - \mu'|$ which still behaves smoothly w.r.t. changes of the mean values and is more informative than $d_{\mathcal{P}^1}^c(\mathcal{D}, \mathcal{D}') = 0$.

The distance function in Eq. (10) is a metric on the set of compactly supported distributions for $k = \infty$, and it is a

pseudo-metric for $k < \infty$ [38]. A zero value of this distance function implies equal moment characteristics. Therefore, it belongs to the class of *primary* probability metrics [49].

VI. PROPERTIES OF THE PROBABILITY METRIC

So far, our approach of defining an appropriate metric, i.e. Eq. (10), has been motivated by theoretical considerations starting from Eq. (1) and the analysis in Section IV. However, for practical applications we need to compute our metric in a computationally efficient way. Theorem 2 provides a key (see Appendix-D for its proof).

Theorem 2: By setting $c_1(\mathcal{D}) = \mathbb{E}_{\mathcal{D}}[\mathbf{x}]$ and $c_k(\mathcal{D}) = \mathbb{E}_{\mathcal{D}}[\boldsymbol{\nu}^{(k)}(\mathbf{x} - \mathbb{E}_{\mathcal{D}}[\mathbf{x}])]$ for $k \geq 2$ with the monomial vector in Eq. (4), we obtain as equivalent representation for the metric in Eq. (10):

$$\text{cmd}_k(\mathcal{D}, \mathcal{D}') = \sum_{j=1}^k a_j \|c_j(\mathcal{D}) - c_j(\mathcal{D}')\|_2. \quad (11)$$

Theorem 2 gives reason to call the metric in Eq. (10) Central Moment Discrepancy.

In the special case of $k = 2$, the sum in Eq. (11) includes the Frobenius norm of the difference between the covariance matrices showing its equivalence to the correlation alignment approaches [15], [31].

It is natural to ask about the difference between the distributions \mathcal{D} and \mathcal{D}' given the value of $\text{cmd}(\mathcal{D}, \mathcal{D}')$. This question is related to the problem of determining a distribution based on its moment sequence, called the moment problem [50]. The moment problem can be uniquely solved for compactly supported distributions (Hausdorff moment problem). For distributions with different support, additional assumptions on the distributions are needed, e.g. Carleman's condition (Hamburger moment problem, Stieltjes moment problem). Under such assumptions, the central moment discrepancy in Eq. (10), together with an error term, can be used to bound the absolute difference between characteristic functions and therefore relates to weak convergence (see Appendix-E for the proofs).

For simplicity let \mathcal{D}_n for $n \in \mathbb{N}$ and \mathcal{D}_∞ be distributions with compact support, zero mean and finite moments of each order. Let further ζ_n and ζ_∞ be the characteristic functions of \mathcal{D}_n and \mathcal{D}_∞ , respectively. Then, $\sup_{\|\mathbf{t}\|_1 \leq 1} |\zeta_n(\mathbf{t}) - \zeta_\infty(\mathbf{t})| \rightarrow 0$ entails weak convergence of the distributions \mathcal{D}_n towards \mathcal{D}_∞ and the following error bound holds.

Theorem 3 (Characteristic Function Bound): For odd $k \in \mathbb{N}$ we have

$$\begin{aligned} \sup_{\|\mathbf{t}\|_1 \leq 1} |\zeta_n(\mathbf{t}) - \zeta_\infty(\mathbf{t})| &\leq \\ &\leq e \text{cmd}_k(\mathcal{D}_n, \mathcal{D}) + \tau(k, \mathcal{D}_n, \mathcal{D}), \end{aligned} \quad (12)$$

where

$$\tau(k, \mathcal{D}_n, \mathcal{D}) = \frac{1}{(k+1)!} \cdot \max_{\|\boldsymbol{\alpha}\|_1 = k+1} (|c_{\boldsymbol{\alpha}}(\mathcal{D}_n)| + |c_{\boldsymbol{\alpha}}(\mathcal{D})|)$$

and the $\boldsymbol{\alpha}$ -moment of \mathcal{D} is given by $c_{\boldsymbol{\alpha}}(\mathcal{D}) = \mathbb{E}_{\mathcal{D}}[x_1^{\alpha_1} \cdots x_m^{\alpha_m}]$ with $\boldsymbol{\alpha} = (\alpha_1, \dots, \alpha_m) \in \mathbb{N}^m$.

Theorem 3 relates the minimization of the CMD to the minimization of the target error in Theorem 1. To see this,

assume that $\tau(k, \mathcal{D}_n, \mathcal{D})$ in Eq. (12) is zero. Then, convergence in CMD implies weak convergence of \mathcal{D}_n to \mathcal{D} . Weak convergence is equivalent to convergence of $\mathbb{E}_{\mathcal{D}_n}[f]$ to $\mathbb{E}_{\mathcal{D}}[f]$ for all bounded continuous functions f . Therefore, if an algorithm forces $\text{cmd}(\mathcal{D}_S, \mathcal{D}_T)$ to tend to zero, it forces also the integral probability metric $d_{\mathcal{F}}(\mathcal{D}_S, \mathcal{D}_T)$ in Theorem 1 to tend to zero for \mathcal{F} being the class of all bounded continuous functions which is assumed to contain $|h - g_S|$ and $|h - g_T|$. Thus, Theorem 1 and Theorem 3 together imply that the algorithm minimizes the target error.

However, the sum in Eq. (12) is only small for very restricted classes of distributions and therefore, Theorem 3 is more of theoretical interest than of practical applicability. Note that, in the one-dimensional case, also lower bounds for Eq. (12) are known for primary probability distances [49, theorem 10.3.6].

In practice, for large k , it is sometimes not useful to compute all cross-moments. Therefore, we reduce the central moment vector in Eq. (4) to

$$\boldsymbol{\nu}^{(k)}(\mathbf{x}) := (x_0^k, \dots, x_m^k). \quad (13)$$

That is, we consider only the marginal central moments in the CMD.

The last theoretical question we have to answer is how to set the weighting factors a_k in Eq. (11) such that the terms of the sum do not increase too much. For distributions with compact support $[a, b]^m$, Proposition 1 provides us with suitable weighting factors, namely $a_k := 1/|b - a|^k$.

Proposition 1 (Upper Central Moment Bound): Let \mathcal{D} and \mathcal{D}' be two compactly supported distributions on $[a, b]^m$ with finite mean values, then

$$\begin{aligned} \frac{1}{|b - a|^k} \|c_k(\mathcal{D}) - c_k(\mathcal{D}')\|_2 \\ \leq 2\sqrt{m} \left(\frac{1}{k+1} \left(\frac{k}{k+1} \right)^k + \frac{1}{2^{1+k}} \right), \end{aligned} \quad (14)$$

where $c_k(\mathcal{D}) = \mathbb{E}_{\mathcal{D}}[\boldsymbol{\nu}^{(k)}(\mathbf{x} - \mathbb{E}_{\mathcal{D}}[\mathbf{x}])]$ is the central moment vector of \mathcal{D} with $\boldsymbol{\nu}^{(k)}$ as defined in Eq. (13).

For $[0, 1]^m$ -supported distributions, Proposition 1 gives some insight in the contribution of lower and higher order central moment terms of the CMD in Eq. (11). The upper bound is strictly decreasing with the order k and shows that higher moment terms can contribute less than lower order moment terms to the overall value of (11). See Appendix-F for the proof of Proposition 1.

VII. DOMAIN ADAPTATION VIA MOMENT ALIGNMENT

We tackle the problem of minimizing the target error of a neural network by minimizing an approximation of the right hand side in the bound of Theorem 1 by means of the minimization of the CMD in Eq. (11) between the domain-specific latent representations. For simplicity, we concentrate on the development of a minimization algorithm for a feed-forward neural network

$$h = h_1 \circ h_0 : \mathbb{R}^m \times \Theta \rightarrow [0, 1]^{|C|} \quad (15)$$

with parameter set Θ and a single hidden layer. The network maps input samples $X \subset \mathbb{R}^m$ to labels $Y \subset [0, 1]^{|C|}$, where Y is an encoding of labels in \mathcal{C} . The first layer (hidden layer) $h_0 : \mathbb{R}^m \times \Theta \rightarrow \mathbb{R}^n$ maps the inputs to the hidden activations $h_0(X) \in \mathbb{R}^n$. The second layer (classification layer) $h_1 : \mathbb{R}^n \times \Theta \rightarrow [0, 1]^{|C|}$ maps the hidden activations to the labels. If it is clear from the application, we use the shorthand notation $h(\mathbf{x}) = h(\mathbf{x}; \Theta)$ and $h(X) = \{h(\mathbf{x})\}_{\mathbf{x} \in X}$ for the sample $X \subset \mathbb{R}^m$.

As hidden layer, we use a standard fully connected layer with non-linear sigmoid activation function, i.e.

$$h_0(\mathbf{x}) = h_0(\mathbf{x}; \mathbf{W}, \mathbf{b}) := \text{sigm}(\mathbf{W}\mathbf{x} + \mathbf{b}) \quad (16)$$

with $\text{sigm}(\mathbf{x}) = \left(\frac{1}{1+e^{-x_1}}, \dots, \frac{1}{1+e^{-x_n}}\right)$ and a matrix-vector parameter pair $\Theta = (\mathbf{W}, \mathbf{b}) \in \mathbb{R}^{n \times m} \times \mathbb{R}^n$.

The classification layer $h_1 : \mathbb{R}^n \times \Theta \rightarrow [0, 1]^{|C|}$ is parametrized by $(\mathbf{V}, \mathbf{c}) \in \mathbb{R}^{|C| \times n} \times \mathbb{R}^{|C|}$ via

$$h_1(\mathbf{x}; \mathbf{V}, \mathbf{c}) := \text{softmax}(\mathbf{V} h_0(\mathbf{x}) + \mathbf{c}) \quad (17)$$

with $\text{softmax}(\mathbf{x}) = (e^{x_1}, \dots, e^{x_{|C|}}) / \sum_{i=1}^{|C|} e^{x_i} \in [0, 1]^{|C|}$. Note that the softmax function enables the interpretation of the output $h(\mathbf{x}) = h_1(h_0(\mathbf{x}))$ as probability vector, i.e. the coordinate $h(\mathbf{x})_i$ can be interpreted as the predicted probability that the vector \mathbf{x} corresponds to the i -th label in \mathcal{C} .

In the following we apply networks of the type in Eq. (15) to the problem of unsupervised domain adaptation as motivated in Section III. Given a labeled source sample $(X_S, Y_S) \subset \mathbb{R}^m \times [0, 1]^{|C|}$ and an unlabeled target sample $X_T \subset \mathbb{R}^m$, we want to train a classifier that performs well on unseen target data. As motivated in Section III-B, this problem can be tackled by training the neural network in Eq. (15) based on the objective

$$\min_{\mathbf{W}, \mathbf{b}, \mathbf{V}, \mathbf{c}} \mathcal{L}(h_1(h_0(X_S; \mathbf{W}, \mathbf{b}); \mathbf{V}, \mathbf{c}), Y_S) + \lambda \cdot d(h_0(X_S; \mathbf{W}, \mathbf{b}), h_0(X_T; \mathbf{W}, \mathbf{b})) \quad (18)$$

with an empirical loss \mathcal{L} in the source domain and a distance function d between the activations $h_0(X_S)$ and $h_0(X_T)$. See Fig. 1 for an illustration. The parameter λ is a trade-off parameter that articulates the priority of the domain adaptation compared to the source error minimization. Objective (18) can be seen as a surrogate for the right hand side in Theorem 1.

A typical choice for the classification loss is the expectation of the negative log probability of the correct label

$$\mathcal{L}(h(X_S), Y_S) := \frac{1}{|(X_S, Y_S)|} \sum_{(\mathbf{x}, \mathbf{y}) \in (X_S, Y_S)} l(h, \mathbf{x}, \mathbf{y}) \quad (19)$$

with $l(h, \mathbf{x}, \mathbf{y}) = -\sum_{i=1}^{|C|} y_i \log(h(\mathbf{x})_i)$ as cross-entropy.

We propose to model the distance function d in Eq. (18) by an empirical estimate of the CMD in Eq. (11) based on

$$\text{cmd}(X_S, X_T) \sim \sum_{j=1}^k \|c_j(X_S) - c_j(X_T)\|_2 \quad (20)$$

with $c_1(X) = \frac{1}{|X|} \sum_{\mathbf{x} \in X} \mathbf{x}$ and $c_k(X) = \frac{1}{|X|} \sum_{\mathbf{x} \in X} \nu^{(k)}(\mathbf{x} - c_1(X))$. According to proposition 1, the weighting factors a_j in Eq. (11) are

set to one as the sigmoid function maps to the interval $[0, 1]$. Note that the estimate in Eq. (20) is consistent but biased [38]. To obtain an unbiased estimate of a moment distance with similar properties as the CMD in Eq. (11), one can apply the sample central moments as unbiased estimates of the central moments and use the squared euclidean norm instead of the euclidean norm in Eq. (11) as similarly proposed for the MMD [20].

We tackle the optimization of Eq. (18) by stochastic gradient descent. Let the objective function be

$$J(\Theta) := \mathcal{L}(h(X_S; \Theta), Y_S) + \lambda \cdot \text{cmd}(X_S, X_T). \quad (21)$$

with the negative log probability $\mathcal{L}(h(X; \Theta), Y)$ as in Eq. (19) and the CMD estimate as in Eq. (20). Then, the gradient update step is given by

$$\Theta^{(k+1)} := \Theta^{(k)} - \alpha \cdot \eta^{(k)} \cdot \nabla_{\Theta} J(\Theta^{(k)}), \quad (22)$$

with learning rate α and gradient weighting $\eta^{(k)}$. The gradients of Eq. (21) are derived in Appendix-G.

In the case of sparse data as in the sentiment analysis experiments in Section VIII-C, we rely on the Adagrad [51] gradient weighting

$$\eta^{(k)} := \frac{1}{\sqrt{G^{(k)}}} \quad (23)$$

$$G^{(k+1)} := G^{(k)} + (\nabla_{\Theta} J(\Theta^{(k)}))^2$$

where the division and the square root are taken element-wise. Eq. (23) can be interpreted as gradient update according to different update weights for each dimension, i.e. the weighting parameter α is divided by the norm of the historical gradient separately for each hidden node. The idea is to give frequently occurring features very low learning rates and infrequent features high learning rates.

In the case of non-sparse, as in the experiments on artificial data in Section VIII-B and in the experiments on image data in Section VIII-D, we use the Adadelta [52] weighting scheme

$$G^{(k)} := \rho G^{(k-1)} + (1 - \rho)(\nabla_{\Theta} J(\Theta^{(k)}))^2$$

$$\eta^{(k)} := \frac{\sqrt{E^{(k-1)} + \epsilon}}{\sqrt{G^{(k)}}} \quad (24)$$

$$E^{(k)} := \rho E^{(k-1)} - (1 - \rho)(\eta^{(k-1)} \cdot \nabla_{\Theta} J(\Theta^{(k)}))^2,$$

where ρ is a decay constant and ϵ is a small number for numerical stability. The Adadelta gradient weighting scheme in Eq. (24) is an extension to the Adagrad gradient weighting scheme in Eq. (23) that seeks to reduce its aggressive, monotonically decreasing learning rate by considering also historical gradient updates $E^{(k)}$. Adadelta requires no manual tuning of a learning rate, i.e. $\alpha = 1$, and appears robust to noisy gradient information, different model architecture choices, various data modalities and selection of hyper-parameters [52]. Adadelta is therefore a suitable choice for our aim of creating a robust learning algorithm.

In our experiments we observe similar scales of the loss function in Eq. (19) and the CMD approximation in Eq. (21). In order to articulate our preference to treat both terms as equally important, it is therefore reasonable to set $\lambda = 1$.

Algorithm 1: Moment Alignment Neural Network - Stochastic Gradient Update

Input: Samples $(X_S, Y_S) \subset \mathbb{R}^m \times [0, 1]^{|C|}$ and $X_T \subset \mathbb{R}^m$
Output: Neural network parameters $\{\mathbf{W}, \mathbf{b}, \mathbf{V}, \mathbf{c}\}$

Init : Initialize parameters $\mathbf{W}, \mathbf{b}, \mathbf{V}$ and \mathbf{c} randomly.
while stopping criteria is not met **do**
 Step 1 : Compute the source activations $h_0(X_S; \mathbf{W}, \mathbf{b})$, the target activations $h_0(X_T; \mathbf{W}, \mathbf{b})$ and the source outputs $h(X_S; \mathbf{W}, \mathbf{b}, \mathbf{V}, \mathbf{c})$ according to Eq. (16) and Eq. (17).
 Step 2 : Compute the gradients of Eq. (21) w.r.t. $\mathbf{W}, \mathbf{b}, \mathbf{V}$ and \mathbf{c} as in Appendix-G.
 Step 3 : Update the parameters $\mathbf{W}, \mathbf{b}, \mathbf{V}$ and \mathbf{c} according to Eq. (22).
end

Let n be the number of hidden nodes of the network, then the gradient update in Step 2 can be implemented with linear time complexity $\mathcal{O}(n \cdot (|X_S| + |X_T|))$ by the formulas derived in Appendix-G. Note that this improves over MMD-based approaches that compute the full kernel matrix and correlation matrix alignment approaches in terms of computational complexity with $\mathcal{O}(n \cdot (|X_S|^2 + |X_S| \cdot |X_T| + |X_T|^2))$ for MMD and $\mathcal{O}(n \cdot |X_S| \cdot |X_T|)$ for correlation alignment approaches.

VIII. EXPERIMENTS

Our experimental evaluations are based on three datasets, one artificial dataset and two benchmark datasets for domain adaptation, *Amazon reviews* and *Office*, described in Subsection VIII-A.

Our experiments aim at providing evidence regarding the following aspects: Subsection VIII-B on the usefulness of our algorithm for adapting neural networks to artificially shifted and rotated data, Subsection VIII-C on the classification accuracy of the proposed algorithm on the sentiment analysis of product reviews, Subsection VIII-D on the classification accuracy on object recognition, and, Subsection VIII-E on the accuracy sensitivity w.r.t. changes of the number of moments parameter and changes of the number of hidden nodes.

A. Datasets

Artificial Dataset: In order to analyse the applicability of our algorithm for adapting neural networks to rotated and shifted data, we created an artificial dataset (Fig. 3). The source data consists of three classes that are arranged in the two-dimensional space. Different transformations such as shifts and rotations are applied on all classes to create unlabeled target data. The dataset is summarized in Table I.

TABLE I: Artificial Dataset

Domain	Nr. samples	Nr. classes	Nr. features
Source	639	3	2
Target	639	3	2

Amazon reviews: For analyzing the accuracy of the proposed approach on sentiment analysis of product reviews, we

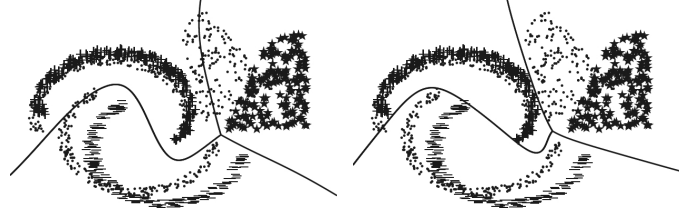


Fig. 3: Artificial classification scenario with three classes (“+”, “-” and stars) in the source domain and unlabeled data in the target domain (points) solved by Algorithm 1. Left: without domain adaptation, i.e. without the cmd-term in Step 2; Right: with the proposed approach.

rely on the *Amazon reviews* benchmark dataset with the same preprocessing as used by [3], [12], [53]. The dataset contains product reviews of four different categories: *books* (B), *DVDs* (D), *electronics* (E) and *kitchen appliances* (K). Reviews are encoded in 5000 dimensional feature vectors of bag-of-words unigrams and bigrams with binary labels: 0 if the product is ranked by 1 – 3 stars and 1 if the product is ranked by 4 or 5 stars. From the four categories we obtain twelve domain adaptation tasks where each category once serves as source domain and once as target domain. The dataset is summarized in Table II.

TABLE II: Amazon Reviews Dataset

Domain	Nr. samples	Nr. classes	Nr. features
Books (B)	6465	2	5000
DVDs (D)	5586	2	5000
Electronics (E)	7231	2	5000
Kitchen appliances (K)	7945	2	5000

Office: In order to analyse the accuracy of our algorithm on an object recognition, we perform experiments based on the *Office* dataset [23] that contains images from three distinct domains: *amazon* (A), *webcam* (W) and *dslr* (D). This dataset is a de facto standard for domain adaptation algorithms in computer vision. We downsample and crop the images such that all are of the same size 227×227 . We assess the performance of our method across all six possible transfer tasks. The dataset is summarized in Table III.

TABLE III: Office Dataset

Domain	Nr. samples	Nr. classes	Nr. features
Amazon (A)	2817	31	227×227
Webcam (W)	795	31	227×227
DSLR (D)	498	31	227×227

B. Artificial Example

The artificial dataset is described in Section VIII-A and visualized in Fig. 3.

We study the adaptation capability of our algorithm by comparing it to a standard neural network described in Section VII with 15 hidden neurons. That is, we apply Algorithm 1 twice, once without the CMD in Eq. (21) and once with the CMD

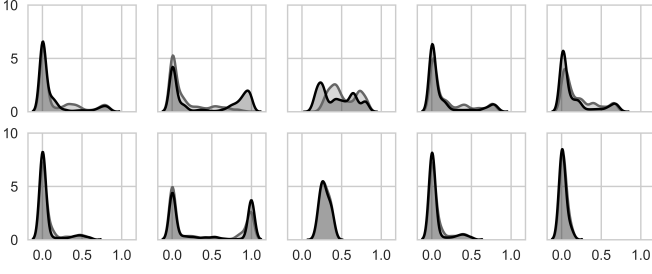


Fig. 4: Five most different source (dark gray) and target (light gray) activation distributions of the hidden nodes of the neural networks trained by Algorithm 1 on the artificial dataset (Fig. 3) without domain adaptation (top) and with the proposed approach (bottom).

term. We refer to the two versions as shallow neural network (shallow NN) and moment alignment neural network (MANN) respectively. To start from a similar initial situation, we use the weights of the shallow NN after $2/3$ of the training time as initial weights for the MANN and train the MANN for $1/3$ of the training time of the shallow NN.

The classification accuracy of the shallow NN in the target domain is 86.7% and the accuracy of the MANN is 99.7%. The decision boundaries of the algorithms are shown in Fig. 3, shallow NN on the left and MANN on the right. It can be seen that the shallow NN misclassifies some data points of the “+”-class and of the star-class in the target domain (points). The MANN clearly adapts the decision boundaries to the target domain. We recall that this is the founding idea of our algorithm.

It is interesting to observe that the MANN misclassifies some points of the class visualized by the “-”. This is no problem as our goal is a high classification accuracy in the target domain and not in the source domain, see Section III.

Let us now test the hypothesis that the CMD helps to align the activation distributions of the hidden nodes. We measure the significance of a distribution difference by means of the p-value of a two-sided Kolmogorov-Smirnov test for goodness of fit. For the shallow NN, 13 out of 15 hidden nodes show significantly different distributions, whereas for the MANN only five distribution pairs are considered as being significantly different (p-value lower than 10^{-2}). Kernel density estimates [54] of these five distribution pairs are visualized in Fig. 4 (bottom). Fig. 4 (top) shows kernel density estimates of the distribution pairs corresponding to the five smallest p-values of the shallow NN. As the only difference between the two algorithms is the CMD, we conclude that the CMD successfully helps to align the activation distributions in this example.

C. Sentiment Analysis of Product Reviews

In the following experiment, we compare our algorithm to related approaches based on the single-layer neural network architecture proposed in Section VII.

We use the Amazon reviews dataset with the same data splits as previous works for every task [3], [12], [53]. Thus, we have 2000 labeled source examples and 2000 unlabeled target

examples for training, and between 3000 and 6000 examples for testing.

Since no target labels are available in the unsupervised domain adaptation setting, it is failed to select parameters through standard cross-validation procedures. Therefore, we apply a variant of the *reverse validation* approach proposed in [55] as refined for neural networks in [3].

We report results for representatives of all three research directions described in Section II and one kernel learning method:

- *Shallow Neural Network (NN)*: Trained by Algorithm 1 without domain adaptation ($\lambda = 0$ in Eq. (21)) on the neural network architecture of Section VII with 50 hidden nodes similarly to [3].
- *Transfer Component Analysis (TCA)* [8]: This kernel learning algorithm tries to learn some transfer components across domains in a RKHS using the MMD. For competitive classification accuracies, we report the results of [9] that search the model architecture in a supervised manner by considering also target labels instead of using unsupervised parameter selection. The trade-off parameter of the TCA is set to $\mu = 0.1$ and the optimal dimension of the subspace is searched for $k \in \{10, 20, \dots, 100, 500\}$.
- *Domain-Adversarial Neural Networks (DANN)* [3]: This algorithm is summarized in Section II. We report the results of the original paper, where the adaptation weighting parameter λ is chosen among 9 values between 10^{-2} and 1 on a logarithmic scale. The hidden layer size is either 50 or 100 and the learning rate is set to 10^{-3} .
- *Deep Correlation Alignment (Coral)* [15]: We apply Algorithm 1 with the CORAL distance function instead of the CMD in Eq. (21). We use the default parameter $\lambda = 1$ as suggested the original paper [15].
- *Maximum Mean Discrepancy (MMD)* [33]: We apply Algorithm 1 with the MMD with Gaussian kernel instead of the CMD in Eq. (21). The parameter λ is chosen among 10 values between 0.1 and 500 on a logarithmic scale. The Gaussian kernel parameter is chosen among 10 values between 0.01 and 10 on a logarithmic scale.
- *Central Moment Discrepancy (CMD)*: The approach of this paper. The number of moments parameter k of the CMD in Eq. (20) is heuristically set to five, as the first five moments capture rich geometric information about the shape of a distribution and $k = 5$ is small enough to be computationally efficient. Note that the experiments in Section VIII-E show that similar results are obtained for all $k \in \{4, \dots, 7\}$.

Since we have to deal with sparse data, we rely on the Adagrad [51] optimization technique in Eq. (23). For all evaluations, the default parametrization is used as implemented in *Keras* [56]. We repeat our experiments ten times with different random initializations.

The mean values and average ranks over all tasks are shown in Table IV. Our method outperforms others in average accuracy as well as in average rank in all except one task.

TABLE IV: Classification accuracy on Amazon reviews dataset for twelve domain adaptation scenarios (source→target)

Method	B→D	B→E	B→K	D→B	D→E	D→K	E→B	E→D	E→K	K→B	K→D	K→E	Average	Average rank
NN	78.7	71.4	74.5	74.6	72.4	76.5	71.1	71.9	84.4	69.9	73.4	83.3	75.2	5.8
DANN [3]	78.4	73.3	77.9	72.3	75.4	78.3	71.3	73.8	85.4	70.9	74.0	84.3	76.3	4.5
CORAL [15]	79.2	73.1	75.0	77.6	74.9	79.2	71.6	72.4	84.5	73.0	75.3	84.0	76.7	4.0
TCA [8]	78.9	74.2	73.9	77.5	77.5	79.6	72.7	75.7	86.6	71.7	74.1	83.5	77.2	3.3
MMD [33]	79.6	75.8	78.7	78.0	76.6	79.6	73.3	74.8	85.7	74.0	76.3	84.4	78.1	2.3
CMD (ours)	80.5	78.7	81.3	79.5	79.7	83.0	74.4	76.3	86.0	75.6	77.5	85.4	79.8	1.1

D. Object Recognition

Since the Office dataset is rather small with only 2817 images in its largest domain, we make use of the pretrained convolutional neural network *AlexNet* [39]. We follow the standard training protocol for this dataset and use the fully labeled source sample and the unlabeled target sample for training [3], [14], [15], [28], [29] and the target labels for testing. Using this “fully-transductive” protocol, we compare the proposed approach to the most related distribution alignment methods described in the last Section VIII-C. For a fair comparison we report original results of papers that align the distributions of a single neural network layer of the AlexNet after the layer called *fc7*. For completeness note that for the Office dataset it was shown recently that the classification accuracy can be further improved by adding multiple layer adaptation or specific knowledge about convolution neural networks structure in the alignment process [28], [29], [37].

We compare our algorithm to the following approaches:

- *Convolutional Neural Network (CNN)* [39]: We apply Algorithm 1 without domain adaptation ($\lambda = 0$ in Eq. (21)) to the network architecture of Section VII on top of the output of the *fc7*-layer of AlexNet. Following [34] and [3] we use a hidden layer size of 256. Following [3], [14] and [28], we randomly crop and mirror the images, ensure a balanced source batch and optimize via stochastic gradient descent with a momentum term of 0.9 and learning rate decay. We set the initial learning rate to 10^{-2} and we apply the default linear decreasing learning rate decay of Keras [56].
- *Transfer Component Analysis (TCA)* [8]: We report the results of [29] that are based on the output of the *fc7*-layer of AlexNet with parameters tuned via reverse validation [55].
- *Domain-Adversarial Neural Networks (DANN)* [3]: In the original paper [3] they report results for the adaptation tasks $A \rightarrow W$, $D \rightarrow W$ and $W \rightarrow D$. For the rest of the scenarios, we report the results of [29]. The distribution alignment is based on a 256-sized layer on top of the *fc7*-layer. The images are randomly cropped and mirrored and stochastic gradient descent is applied with a momentum term of 0.9. The learning rate is decreased polynomially and divided by ten for the lower layers. It is proposed to decrease the weighting parameter λ in Eq. (18) with exponential order according to a specifically designed λ -schedule.
- *Deep Correlation Alignment (Coral)* [15]: We report the results and parameters of the original paper in which they

perform domain adaptation on a 31-sized layer on top of the *fc7*-layer. Stochastic gradient descent is applied with a learning rate of 10^{-3} , weight decay of $5 \cdot 10^{-4}$ and momentum of 0.9. The domain adaptation weighting parameter λ is chosen in such a way that “at the end of training the classification loss and the CORAL loss are roughly the same” [15].

- *Maximum Mean Discrepancy (MMD)* [33]: We report the results of [14] in which the MMD is applied on top of the 31-dimensional layer after the *fc7*-layer. The domain adaptation weighting parameter λ is chosen based on assessing the error of a two-sample classifier according to [57]. In this work, a multi-kernel version of the MMD is used with varying bandwidth of the Gaussian kernel between $2^{-8}\gamma$ and $2^8\gamma$ with multiplicative step-size of $\sqrt{2}$. γ is chosen as the median pairwise distance on the training data, i.e. the *median heuristic* [58]. The network is trained via stochastic gradient descent with momentum of 0.9 and polynomial learning rate decay and cross-validated initial learning rate between 10^{-5} and 10^{-2} with multiplicative step size of $\sqrt{10}$. The learning rate is set to zero for the first three layers and for the lower layers it is divided by 10. The images are randomly cropped and mirrored in this approach to stabilize the learning process.
- *Central Moment Discrepancy (CMD)*: The approach of this paper with the same optimization strategy as of CNN and the number of moments parameter $k = 5$ as described in the last Section VIII-C.
- *Few Parameter Central Moment Discrepancy (FP-CMD)*: The Adadelta gradient weighting scheme (Eq. (24)) is used instead of the momentum in the method before. In addition, no data augmentation is applied.

The parameter settings of the neural network based approaches are summarized in Table V.

We repeated all evaluation five times with different random initializations and report the average accuracies and average ranks over all tasks in Table VI.

Without considering the Robust-CMD implementation, the CMD implementation shows the highest accuracy in four of six domain adaptation tasks on this dataset. In the last two tasks, the DANN algorithm shows the highest accuracy which also has the highest average accuracy due to these two scenarios.

The Robust-CMD implementation shows the highest accuracy in three of six tasks over all approaches and achieves the best average rank. In contrast to the other approaches, this is achieved without data mirroring or rotation, no tuned, manually decreasing or cross-validated learning rates, no dif-

TABLE V: Summary of parameter settings of state-of-the-art neural network approaches as applied on the Office dataset.

Method	Adaptation Nodes	Adaptation Weight λ	Additional Hyper-Parameters	Gradient Weighting η	Learn. Rate	Learn. Rate Decay	Data Augmentation	Weight Decay
CORAL [15]	31	manually tuned	no	momentum	10^{-3}	no	yes	yes
DANN [3]	256	exp. decay	additional classifier	momentum	10^{-3}	yes	yes	no
MMD [14], [33]	31	class. strategy	range of kernel parameters	momentum	cv	yes	yes	no
CMD (ours)	256	1.0	$k = 5$	momentum	10^{-2}	yes	yes	no
FP-CMD (ours)	256	1.0	$k = 5$	adadelata	no	no	no	no

TABLE VI: Classification accuracy on Office dataset for six domain adaptation scenarios (source→target)

Method	A→W	D→W	W→D	A→D	D→A	W→A	Average	Average rank
CNN [39]	52.9	94.7	99.0	62.5	50.2	48.1	67.9	6.3
TCA [8]	61.0	95.4	95.2	60.8	51.6	50.9	69.2	6.0
MMD [14], [33]	63.8	94.6	98.8	65.8	52.8	51.9	71.3	4.7
CORAL [15]	66.4	95.7	99.2	66.8	52.8	51.5	72.1	3.2
DANN [3]	73.0	96.4	99.2	72.3	53.4	51.2	74.3	2.5
CMD (ours)	62.8	96.7	99.3	66.0	53.6	51.9	71.7	2.7
FP-CMD (ours)	64.8	95.4	99.4	67.0	55.1	53.5	72.5	2.0

ferent learning rates for different layers and without tuning the domain adaptation weighting parameter λ in Eq. (18).

The next section analyses the accuracy sensitivity w.r.t. changes of the hidden layer size and the number of moments parameter.

E. Accuracy Sensitivity w.r.t. Parameter Changes

The first sensitivity experiment aims at providing evidence regarding the accuracy sensitivity of the CMD regularizer w.r.t. parameter changes of the number of moments parameter k . That is, the contribution of higher terms in the CMD are analysed. The claim is that the accuracy of CMD-based networks does not depend strongly on the choice of k in a range around its default value 5.

In Fig. 5 we analyse the classification accuracy of a CMD-based network trained on all tasks of the Amazon reviews experiment. We perform a grid search for the number of moments parameter k and the standard weighting parameter λ in the objective in Eq. (21). We empirically choose a representative stable region for each parameter, $[0.3, 3]$ for λ and $\{1, \dots, 7\}$ for k . Since we want to analyse the sensitivity w.r.t. k , we averaged over the λ -dimension, resulting in one accuracy value per k for each of the 12 tasks. Each accuracy is transformed into an accuracy ratio value by dividing it by the accuracy of $k = 5$. Thus, for each k and each task, we get one value representing the ratio between the obtained accuracy and the accuracy of $k = 5$. The results are shown in Fig. 5 on the upper left. The accuracy ratios between $k = 5$ and $k \in \{3, 4, 6, 7\}$ are lower than 0.5%, which underpins the claim that the accuracy of CMD-based networks does not depend strongly on the choice of k in a range around its default value 5. For $k = 1$ and $k = 2$ higher ratio values are obtained. In addition, for these two values many tasks show worse accuracy than obtained by $k \in \{3, 4, 5, 6, 7\}$. From this we additionally conclude that higher values of k are preferable to $k = 1$ and $k = 2$.

The same experimental procedure is performed with MMD regularization weighted by $\lambda \in [5, 45]$ and Gaussian kernel parameter $\beta \in [0.3, 1.7]$. We calculate the ratio values w.r.t. the accuracy of $\beta = 1.2$, since this value of β shows the highest mean accuracy of all tasks. Fig. 5 on the upper right shows the results. It can be seen that the accuracy of the MMD network is more sensitive to parameter changes than the CMD optimized version. Note that the problem of finding the best settings for the parameter β of the Gaussian kernel is a well known problem [59].

The default number of hidden nodes in the sentiment analysis experiments in Section VIII-D is 50 to be comparable with other state-of-the-art approaches [3]. The question arises if the accuracy of the CMD is lower for higher numbers of hidden nodes. That is, if the accuracy ratio in Table IV between the accuracy of the CMD-based networks compared to the accuracy of the NN models decreases with increasing hidden activation dimension. In order to answer this question we calculate these ratio values for each task of the Amazon reviews dataset for different numbers of hidden nodes in $\{128, 256, 384, \dots, 1664\}$. For higher numbers of hidden nodes our NN models don't converge with the optimization settings under consideration. For the parameters λ and k we use our default setting $\lambda = 1$ and $k = 5$. Fig. 5 on the lower left shows the ratio values (vertical axis) for every number of hidden nodes (horizontal axis) and every task (colored lines). It can be seen that the accuracy improvement of the CMD domain regularizer varies between 4% and 6%. However, no significant accuracy ratio decrease can be observed.

Fig. 5 shows that our default setting ($\lambda = 1, k = 5$) can be used independently of the number of hidden nodes for the sentiment analysis task.

The same procedure is performed with the MMD weighted by parameter $\lambda = 9$ and $\beta = 1.2$ as these values show the highest classification accuracy for 50 hidden nodes. Fig. 5 on the lower right shows that the accuracy improvement using

the MMD decreases with increasing number of hidden nodes for this parameter setting. That is, for accurate performance of the MMD, additional parameter tuning procedures for λ and β need to be performed.

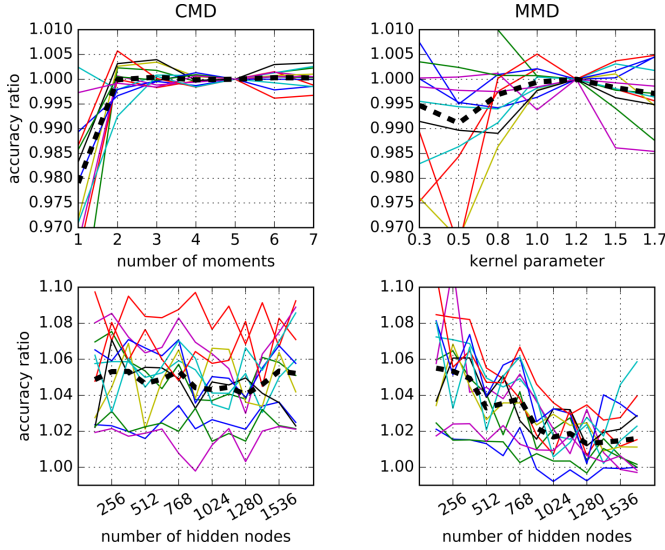


Fig. 5: Sensitivity of classification accuracy w.r.t. different parameters of CMD (left) and MMD (right) on the Amazon reviews dataset. The horizontal axes show parameter values and the vertical axes show accuracy ratio values. Each line in the plots represents accuracy ratio values for one specific task. The ratio values on the upper left are computed w.r.t. the default accuracy for CMD ($k = 5$) and on the right w.r.t. the best obtainable accuracy for MMD ($\beta = 1.2$). The ratio values in the lower column are computed w.r.t. the accuracies of the networks with the same hidden layer but without domain adaptation.

IX. CONCLUSION

We proposed a novel approach for unsupervised domain-adaptation for neural networks that relies on a metric-based regularization of the learning process. The regularization aims at maximizing the similarity of domain-specific activation distributions by minimizing the proposed Central Moment Discrepancy (CMD) metric. The CMD solves instability issues that arise in the application of integral probability metrics based on polynomial reproducing kernel Hilbert spaces. We theoretically proved further appealing properties of the CMD including a relation to weak convergence of distributions, a strictly decreasing upper bound for its moment terms and a computationally efficiently implementable dual representation. We empirically analysed the classification performance of the CMD on an artificial and two benchmark datasets for domain adaptation. It turns out that the proposed approach is robust w.r.t. theoretical and practical aspects while it shows higher classification accuracies than comparable state-of-the-art approaches on most domain adaptation tasks on standard benchmark datasets for sentiment analysis of product reviews and object recognition.

APPENDIX

A. Proof of Theorem 1

Note that

$$\begin{aligned} \epsilon_T(h, g_T) &\leq \epsilon_S(h, g_S) + |\epsilon_S(h, g_T) - \epsilon_S(h, g_S)| \\ &\quad + |\epsilon_T(h, g_T) - \epsilon_S(h, g_T)| \\ &\leq \epsilon_S(h, g_S) + \mathbb{E}_{\mathcal{D}_S}[|g_S - g_T|] \\ &\quad + \left| \int_{\mathcal{X}} |h - g_T| d\mathcal{D}_S - \int_{\mathcal{X}} |h - g_T| d\mathcal{D}_T \right|. \end{aligned}$$

By adding and subtracting $\epsilon_T(h, g_S)$ instead of $\epsilon_S(h, g_T)$ we get

$$\begin{aligned} \epsilon_T(h) &\leq \epsilon_S(h) + \mathbb{E}_{\mathcal{D}_T}[|g_S - g_T|] \\ &\quad + \left| \int_{\mathcal{X}} |h - g_S| d\mathcal{D}_S - \int_{\mathcal{X}} |h - g_S| d\mathcal{D}_T \right| \end{aligned}$$

By taking the minimum of the two bounds and the supremum of the last term the required result is obtained ■

B. Proof of RKHS Property (6)

The proof has three main components: the proof of κ being a positive definite kernel, the construction of a RKHS \mathcal{H} with κ as reproducing kernel and unit ball \mathcal{P} , and the proof of the uniqueness of \mathcal{H} .

For all $n \in \mathbb{N}$, $c_1, \dots, c_n \in \mathbb{R}$ and $\mathbf{x}_1, \dots, \mathbf{x}_n \in \mathbb{R}^m$ it holds that

$$\begin{aligned} \sum_{i=1}^n \sum_{j=1}^n c_i c_j \kappa(\mathbf{x}_i, \mathbf{x}_j) &= \sum_{i=1}^n \sum_{j=1}^n c_i c_j \langle \boldsymbol{\nu}(\mathbf{x}_i), \boldsymbol{\nu}(\mathbf{x}_j) \rangle_2 \\ &= \left\langle \sum_{i=1}^n c_i \boldsymbol{\nu}(\mathbf{x}_i), \sum_{j=1}^n c_j \boldsymbol{\nu}(\mathbf{x}_j) \right\rangle_2 \\ &= \left\| \sum_{i=1}^n c_i \boldsymbol{\nu}(\mathbf{x}_i) \right\|_2^2 \geq 0. \end{aligned}$$

Let us define $\mathcal{H} := \text{span}\{\kappa(\mathbf{x}, \cdot) | \mathbf{x} \in \mathbb{R}^m\}$ and note that $\mathcal{H} = \{\langle \mathbf{w}, \boldsymbol{\nu}(\cdot) \rangle_2 | \mathbf{w} \in \mathbb{R}^{\dim(\boldsymbol{\nu}(\mathbf{x}))}\}$. Define the inner product $\langle \cdot, \cdot \rangle_{\mathcal{H}}$ on \mathcal{H} by $\langle \langle \mathbf{w}, \boldsymbol{\nu}(\cdot) \rangle_2, \langle \mathbf{w}', \boldsymbol{\nu}(\cdot) \rangle_2 \rangle_{\mathcal{H}} := \langle \mathbf{w}, \mathbf{w}' \rangle_2$. The polynomial space \mathcal{H} with the above inner product is a Hilbert space, as convergence of sequences in this space can be identified by the convergence of the respective coefficient vectors $\mathbf{w} \in \mathbb{R}^{\dim(\boldsymbol{\nu}(\mathbf{x}))}$. For all $f = \langle \mathbf{w}, \boldsymbol{\nu}(\cdot) \rangle_2 \in \mathcal{H}$ the reproducing property holds, i.e. $\langle f, \kappa(\mathbf{x}, \cdot) \rangle_{\mathcal{H}} = \langle \langle \mathbf{w}, \boldsymbol{\nu}(\cdot) \rangle_2, \kappa(\mathbf{x}, \cdot) \rangle_{\mathcal{H}} = \langle \mathbf{w}, \boldsymbol{\nu}(\mathbf{x}) \rangle_2 = f(\mathbf{x})$. The unit ball of \mathcal{H} is given by \mathcal{P} in Eq. (5).

The uniqueness of \mathcal{H} is given by the Moore-Aronszajn theorem [48].

C. An Example of Mean Over-Penalization

Let the source distribution \mathcal{D}_S be defined by the random variable $X_S = 0.8Y + 0.1$ with Y following a Beta distribution with shape parameters $\alpha = \beta = 0.4$ (Fig. 2 dashed). Let the left target distribution $\mathcal{D}_T^{(L)}$ be a Normal distribution with mean 0.5 and variance 0.27² (Fig. 2 left) and let the right

target distribution $\mathcal{D}_T^{(R)}$ be defined by the random variable $X_T = 0.8 \cdot Y + 0.12$ (Fig. 2 right). Then,

$$\begin{aligned} d_{\mathcal{P}^1}(\mathcal{D}_S, \mathcal{D}_T^{(L)}) &= |\mathbb{E}_{\mathcal{D}_S}[x] - \mathbb{E}_{\mathcal{D}_T^{(L)}}[x]| \\ &= 0 < 0.02 < d_{\mathcal{P}^1}(\mathcal{D}_S, \mathcal{D}_T^{(R)}), \end{aligned}$$

and for \mathcal{P}^2 and \mathcal{P}^4 it follows

$$\begin{aligned} d_{\mathcal{P}^2}(\mathcal{D}_S, \mathcal{D}_T^{(L)}) &< 0.016 < 0.02 < d_{\mathcal{P}^2}(\mathcal{D}_S, \mathcal{D}_T^{(R)}) \\ d_{\mathcal{P}^4}(\mathcal{D}_S, \mathcal{D}_T^{(L)}) &< 0.02 < 0.021 < d_{\mathcal{P}^4}(\mathcal{D}_S, \mathcal{D}_T^{(R)}). \end{aligned}$$

Let us now consider the MMD [22], [33] with standard polynomial kernel $\kappa_2(x, y) = (1 + xy)^2$. It holds that

$$\begin{aligned} \text{MMD}_{\kappa_2}(\mathcal{D}_S, \mathcal{D}_T^{(L)}) &= \\ &= \mathbb{E}_{\mathcal{D}_S}[\mathbb{E}_{\mathcal{D}_S}[\kappa(x, x')]] + \mathbb{E}_{\mathcal{D}_T^{(L)}}[\mathbb{E}_{\mathcal{D}_T^{(L)}}[\kappa(y, y')]] \\ &\quad - 2\mathbb{E}_{\mathcal{D}_S}[\mathbb{E}_{\mathcal{D}_T^{(L)}}[\kappa(x, y)]] \\ &= 2|\mathbb{E}_{\mathcal{D}_S}[x] - \mathbb{E}_{\mathcal{D}_T^{(L)}}[x]|^2 + |\mathbb{E}_{\mathcal{D}_S}[x^2] - \mathbb{E}_{\mathcal{D}_T^{(L)}}[x^2]|^2 \\ &< 0.00025 < 0.0012 < \text{MMD}_{\kappa_2}(\mathcal{D}_S, \mathcal{D}_T^{(R)}). \end{aligned}$$

Similarly it follows for the cubic kernel $\kappa_4(x, y) = (1 + xy)^4$ that

$$\text{MMD}_{\kappa_4}(\mathcal{D}_S, \mathcal{D}_T^{(L)}) < 0.004 < 0.006 < \text{MMD}_{\kappa_4}(\mathcal{D}_S, \mathcal{D}_T^{(R)}).$$

The mean and covariance feature matching integral probability metrics in [21] coincide in our example with the integral probability metrics based on \mathcal{P}^1 and \mathcal{P}^2 . Finally, for the CMD in Eq. (10) with $a_1 = \dots = a_4 = 1$, we obtain

$$\text{cmd}_4(\mathcal{D}_S, \mathcal{D}_T^{(L)}) > 0.0207 > 0.02 > \text{cmd}_4(\mathcal{D}_S, \mathcal{D}_T^{(R)}).$$

D. Proof of Theorem 2

The proof follows from the linearity of the expectation and the duality of norms in the Hilbert space \mathcal{H} defined in Appendix-B. It holds that

$$\begin{aligned} \text{cmd}_k(\mathcal{D}, \mathcal{D}') &= \\ &= \sup_{f \in \mathcal{P}^1} |\mathbb{E}_{\mathcal{D}}[f] - \mathbb{E}_{\mathcal{D}'}[f]| \\ &\quad + \sum_{j=2}^k \sup_{f \in \mathcal{P}^j} |\mathbb{E}_{\mathcal{D}}[f(\mathbf{x} - \mathbb{E}_{\mathcal{D}}[\mathbf{x}])] - \mathbb{E}_{\mathcal{D}'}[f(\mathbf{x} - \mathbb{E}_{\mathcal{D}'}[\mathbf{x}])]| \\ &= \sup_{\|\mathbf{w}\|_2 \leq 1} |\mathbb{E}_{\mathcal{D}}[\langle \mathbf{w}, \mathbf{x} \rangle_2] - \mathbb{E}_{\mathcal{D}'}[\langle \mathbf{w}, \mathbf{x} \rangle_2]| \\ &\quad + \sum_{j=2}^k \sup_{\|\mathbf{w}\|_2 \leq 1} |\mathbb{E}_{\mathcal{D}}[\langle \mathbf{w}, \boldsymbol{\nu}^{(j)}(\mathbf{x} - \mathbb{E}_{\mathcal{D}}[\mathbf{x}]) \rangle_2] \\ &\quad - \mathbb{E}_{\mathcal{D}'}[\langle \mathbf{w}, \boldsymbol{\nu}^{(j)}(\mathbf{x} - \mathbb{E}_{\mathcal{D}'}[\mathbf{x}]) \rangle_2]| \\ &= \sup_{\|\mathbf{w}\|_2 \leq 1} |\langle \mathbf{w}, \mathbb{E}_{\mathcal{D}}[\mathbf{x}] - \mathbb{E}_{\mathcal{D}'}[\mathbf{x}] \rangle_2| \\ &\quad + \sum_{j=2}^k \sup_{\|\mathbf{w}\|_2 \leq 1} |\langle \mathbf{w}, \mathbb{E}_{\mathcal{D}}[\boldsymbol{\nu}^{(j)}(\mathbf{x} - \mathbb{E}_{\mathcal{D}}[\mathbf{x}])] \\ &\quad - \mathbb{E}_{\mathcal{D}'}[\boldsymbol{\nu}^{(j)}(\mathbf{x} - \mathbb{E}_{\mathcal{D}'}[\mathbf{x}])] \rangle_2|, \end{aligned}$$

and finally $\text{cmd}_k(\mathcal{D}, \mathcal{D}') = \sum_{j=1}^k \|c_j(\mathcal{D}) - c_j(\mathcal{D}')\|_2$ ■

E. Proof of Theorem 3

We use the multi-index notations $\mathbf{t}^\alpha = t_1^{\alpha_1} \dots t_m^{\alpha_m}$, $\alpha! = \alpha_1! \dots \alpha_m!$, $\mathbf{D}^\alpha = D_1^{\alpha_1} \dots D_m^{\alpha_m}$ and $|\alpha| = \alpha_1 + \dots + \alpha_m$.

Since all moments $c_\alpha(\mathcal{D})$ are finite, the characteristic functions ζ_n, ζ_∞ are analytic. Note that $c_\alpha(\mathcal{D}_n) = (-i)^{|\alpha|} \mathbf{D}^\alpha \zeta_n(\mathbf{t})|_{\mathbf{t}=0}$ and therefore,

$$\begin{aligned} \zeta_n(\mathbf{t}) &= \mathbb{E}_{\mathcal{D}_n}[e^{i\langle \mathbf{t}, \mathbf{x} \rangle}] \\ &= \sum_{|\alpha| \geq 1} \frac{\mathbf{t}^\alpha}{\alpha!} \mathbb{E}_{\mathcal{D}_n}[\mathbf{D}^\alpha \zeta_n(\mathbf{0})] \\ &= \sum_{|\alpha| \geq 1} \frac{(-i)^{|\alpha|} c_\alpha(\mathcal{D}_n)}{\alpha!} \mathbf{t}^\alpha \\ &= \sum_{|\alpha| \leq k} \frac{(-i)^{|\alpha|} c_\alpha(\mathcal{D}_n)}{\alpha!} \mathbf{t}^\alpha + \sum_{|\alpha| = k+1} \frac{\mathbf{t}^\alpha}{\alpha!} \mathbf{D}^\alpha \zeta_n(\xi \cdot \mathbf{t}) \end{aligned}$$

for some $\xi \in (0, 1)$ by Taylor's formula with Lagrange's form of the remainder.

Let k be odd, i.e., $|\alpha| = k+1$ is even. Then, by integration and $|e^{i\langle \mathbf{t}, \mathbf{x} \rangle}| \leq 1$ it follows that $\mathbf{D}^\alpha \zeta_n(\xi \cdot \mathbf{t}) \leq c_\alpha(\mathcal{D}_n)$ and therefore,

$$\begin{aligned} |\zeta_n(\mathbf{t}) - \zeta_\infty(\mathbf{t})| &\leq \sum_{|\alpha| \leq k} \frac{|c_\alpha(\mathcal{D}_n) - c_\alpha(\mathcal{D}_\infty)|}{\alpha!} \mathbf{t}^\alpha \\ &\quad + \sum_{|\alpha| = k+1} \frac{\mathbf{t}^\alpha}{\alpha!} (|c_\alpha(\mathcal{D}_n)| + |c_\alpha(\mathcal{D}_\infty)|) \\ &\leq e^{\|\mathbf{t}\|_1} \cdot \text{cmd}(\mathcal{D}_n, \mathcal{D}_\infty) \\ &\quad + \frac{\|\mathbf{t}\|_1^{k+1}}{(k+1)!} \cdot \max_{|\alpha| = k+1} (|c_\alpha(\mathcal{D}_n)| + |c_\alpha(\mathcal{D}_\infty)|) \end{aligned}$$

for all $\|\mathbf{t}\|_1 \leq 1$.

The characteristic functions ζ_n are analytic and thus, the uniform convergence on the unit interval implies pointwise convergence on \mathbb{R}^m . The weak convergence of the distributions follows from Levy's continuity theorem in multiple dimensions [43, Theorem 9.8.2] ■

F. Proof of Proposition 1

Note that

$$\begin{aligned} \frac{1}{|b-a|^k} \|c_k(\mathcal{D}) - c_k(\mathcal{D}')\|_2 &\leq \\ &\leq 2\sqrt{m} \max_{\mathcal{D} \in \mathcal{C}[a,b]} \left| \frac{c_k(\mathcal{D})}{(b-a)^k} \right| \\ &\leq 2\sqrt{m} \max_{\mathcal{D} \in \mathcal{C}[a,b]} \mathbb{E}_{\mathcal{D}} \left[\left| \frac{x - \mathbb{E}_{\mathcal{D}}[x]}{b-a} \right|^k \right] \end{aligned}$$

where $\mathcal{C}[a, b]$ is the set of all one-dimensional $[a, b]$ -supported distributions. By applying the Edmundson-Mandansky in-

equality [60] to the convex function $|(x - \mathbb{E}_{\mathcal{D}}[x])/(b - a)|^k$ and symmetry arguments as in [61], we get

$$\begin{aligned} \mathbb{E}_{\mathcal{D}} \left[\left| \frac{x - \mathbb{E}_{\mathcal{D}}[x]}{b - a} \right|^k \right] &\leq \frac{b - \mathbb{E}_{\mathcal{D}}[x]}{b - a} \cdot \left| \frac{a - \mathbb{E}_{\mathcal{D}}[x]}{b - a} \right|^k \\ &\quad + \frac{\mathbb{E}_{\mathcal{D}}[x] - a}{b - a} \cdot \left| \frac{b - \mathbb{E}_{\mathcal{D}}[x]}{b - a} \right|^k \\ &\leq \max_{x \in [0,1]} ((1-x)x^k + (1-x)^k x) \\ &= \max_{x \in [0,1/2]} ((1-x)x^k + (1-x)^k x) \\ &\leq \max_{x \in [0,1/2]} (1-x)x^k + \max_{x \in [0,1/2]} (1-x)^k x \\ &\leq \frac{1}{k+1} \left(\frac{k}{k+1} \right)^k + \frac{1}{2^{1+k}} \blacksquare \end{aligned}$$

G. Derivation of Gradients

Here, we derive the gradients of the CMD estimate in Eq. (20) for the neural network architecture in Section VII. Let the mean $\mathbb{E}[X]$ of the sample X be defined by $\mathbb{E}[X] = \frac{1}{|X|} \sum_{\mathbf{x} \in X} \mathbf{x}$ and the sampled central moments $\mathbb{E}[\nu^{(k)}(X - \mathbb{E}[X])]$, with the set notations

$$\begin{aligned} X - \mathbb{E}[X] &:= \{\mathbf{x} - \mathbb{E}[X] | \mathbf{x} \in X\}, \\ \nu^{(k)}(X) &:= \{\nu^{(k)}(\mathbf{x}) | \mathbf{x} \in X\}. \end{aligned}$$

Let \odot be the coordinate-wise multiplication. Then, by setting

$$\begin{aligned} \nabla_{\mathbf{b}} \text{cmd} &:= \nabla_{\mathbf{b}} \text{cmd}(h_0(X_S), h_0(X_T)), \\ \nabla_{\mathbf{W}} \text{cmd} &:= \nabla_{\mathbf{W}} \text{cmd}(h_0(X_S), h_0(X_T)), \\ \mathbf{\Gamma}_{j,X} &:= \nu^{(j)}(h_0(X) - \mathbb{E}[h_0(X)]), \\ \Delta_{X_S, X_T} &:= h_0(X_S) - h_0(X_T), \\ \mathbf{q}_X &:= h_0(X) \odot (\mathbf{1} - h_0(X)), \end{aligned}$$

the application of the chain rule gives

$$\begin{aligned} \nabla_{\mathbf{b}} \text{cmd} &= \nabla_{\mathbf{b}} \|\mathbb{E}[\Delta_{X_S, X_T}]\|_2 \\ &\quad + \sum_{j=2}^k \nabla_{\mathbf{b}} \|\mathbb{E}[\mathbf{\Gamma}_{j, X_S}] - \mathbb{E}[\mathbf{\Gamma}_{j, X_T}]\|_2 \\ &= \frac{\mathbb{E}[\Delta_{X_S, X_T}] \odot (\mathbb{E}[\mathbf{q}_{X_S}] - \mathbb{E}[\mathbf{q}_{X_T}])}{\|\mathbb{E}[\Delta_{X_S, X_T}]\|_2} \\ &\quad + \sum_{j=2}^k \frac{\mathbb{E}[\mathbf{\Gamma}_{j, X_S}] - \mathbb{E}[\mathbf{\Gamma}_{j, X_T}]}{\|\mathbb{E}[\mathbf{\Gamma}_{j, X_S}] - \mathbb{E}[\mathbf{\Gamma}_{j, X_T}]\|_2} \\ &\quad \odot (\mathbb{E}[\nabla_{\mathbf{b}} \mathbf{\Gamma}_{j, X_S}] - \mathbb{E}[\nabla_{\mathbf{b}} \mathbf{\Gamma}_{j, X_T}]) \end{aligned}$$

and

$$\nabla_{\mathbf{b}} \mathbf{\Gamma}_{j, X} = j \cdot \mathbf{\Gamma}_{j-1, X} \odot (\mathbf{q}_X - \mathbb{E}[\mathbf{q}_X]),$$

which follows from

$$\nabla_{\mathbf{x}} \text{sigm}(\mathbf{x}) = \text{sigm}(\mathbf{x}) \odot (\mathbf{1} - \text{sigm}(\mathbf{x})).$$

Analogously, we obtain $\nabla_{\mathbf{W}} \text{cmd}$.

The gradients of the cross-entropy loss function w.r.t. \mathbf{W} , \mathbf{b} , \mathbf{V} and \mathbf{c} are

$$\begin{aligned} \nabla_{\mathbf{c}} \mathcal{L}(h(X_S), Y_S) &= \mathbb{E}[h_1(X_S) - Y_S], \\ \nabla_{\mathbf{V}} \mathcal{L}(h(X_S), Y_S) &= \mathbb{E}[(h_1(X_S) - Y_S) \cdot h_1(X_S)^T], \\ \nabla_{\mathbf{b}} \mathcal{L}(h(X_S), Y_S) &= \mathbb{E}[\mathbf{V}^T (h_1(X_S) - Y_S) \\ &\quad \odot h_1(X) \odot (\mathbf{1} - h_1(X))], \\ \nabla_{\mathbf{W}} \mathcal{L}(h(X_S), Y_S) &= \mathbb{E}[(\mathbf{V}^T (h_1(X_S) - Y_S) \odot h_1(X) \\ &\quad \odot (\mathbf{1} - h_1(X))) \cdot X_S^T]. \end{aligned}$$

REFERENCES

- [1] X. Glorot, A. Bordes, and Y. Bengio, "Domain adaptation for large-scale sentiment classification: A deep learning approach," in *International Conference on Machine Learning*, pp. 513–520, 2011.
- [2] B. Sun and K. Saenko, "From virtual to reality: Fast adaptation of virtual object detectors to real domains," in *British Machine Vision Conference*, 2014.
- [3] Y. Ganin, E. Ustinova, H. Ajakan, P. Germain, H. Larochelle, F. Laviolette, M. Marchand, and V. Lempitsky, "Domain-adversarial training of neural networks," *Journal of Machine Learning Research*, vol. 17, no. Jan, pp. 1–35, 2016.
- [4] W. Zellinger and B. Moser, "Improving visual discomfort prediction for stereoscopic images via disparity-based contrast," *Journal of Imaging Science and Technology*, vol. 60, no. 1, pp. 1–8, 2016.
- [5] W. Zellinger, B. Moser, A. Chouikhi, F. Seitner, M. Nezveda, and M. Gelautz, "Linear optimization approach for depth range adaption of stereoscopic videos," *Stereoscopic Displays and Applications XXVII, IS&T Electronic Imaging*, 2016.
- [6] J. Blitzer, R. McDonald, and F. Pereira, "Domain adaptation with structural correspondence learning," in *Conference on Empirical Methods in Natural Language Processing*, pp. 120–128, Association for Computational Linguistics, 2006.
- [7] S. J. Pan and Q. Yang, "A survey on transfer learning," *IEEE Transactions on Knowledge and Data Engineering*, vol. 22, no. 10, pp. 1345–1359, 2010.
- [8] S. J. Pan, I. W. Tsang, J. T. Kwok, and Q. Yang, "Domain adaptation via transfer component analysis," *IEEE Transactions on Neural Networks*, vol. 22, no. 2, pp. 199–210, 2011.
- [9] S. Li, S. Song, and G. Huang, "Prediction reweighting for domain adaptation," *IEEE Transactions on Neural Networks and Learning Systems*, 2017.
- [10] S. Ben-David, J. Blitzer, K. Crammer, A. Kulesza, F. Pereira, and J. W. Vaughan, "A theory of learning from different domains," *Machine learning*, vol. 79, no. 1–2, pp. 151–175, 2010.
- [11] S. J. Pan, X. Ni, J.-T. Sun, Q. Yang, and Z. Chen, "Cross-domain sentiment classification via spectral feature alignment," in *International Conference on World Wide Web*, pp. 751–760, ACM, 2010.
- [12] M. Chen, Z. Xu, K. Weinberger, and F. Sha, "Marginalized denoising autoencoders for domain adaptation," *International Conference on Machine Learning*, pp. 767–774, 2012.
- [13] K. Zhang, V. Zheng, Q. Wang, J. Kwok, Q. Yang, and I. Marsic, "Covariate shift in hilbert space: A solution via surrogate kernels," in *International Conference on Machine Learning*, pp. 388–395, 2013.
- [14] M. Long, Y. Cao, J. Wang, and M. Jordan, "Learning transferable features with deep adaptation networks," in *Proceedings of the International Conference on Machine Learning*, pp. 97–105, 2015.
- [15] B. Sun and K. Saenko, "Deep coral: Correlation alignment for deep domain adaptation," in *Computer Vision—ECCV 2016 Workshops*, pp. 443–450, Springer, 2016.
- [16] Y. LeCun, Y. Bengio, and G. Hinton, "Deep learning," *Nature*, vol. 521, no. 7553, pp. 436–444, 2015.
- [17] Y. Bengio, A. Courville, and P. Vincent, "Representation learning: A review and new perspectives," *IEEE Transactions on Pattern Analysis and Machine Intelligence*, vol. 35, no. 8, pp. 1798–1828, 2013.
- [18] A. Müller, "Integral probability metrics and their generating classes of functions," *Advances in Applied Probability*, vol. 29, no. 2, pp. 429–443, 1997.

- [19] B. K. Sriperumbudur, A. Gretton, K. Fukumizu, B. Schölkopf, and G. R. Lanckriet, "Hilbert space embeddings and metrics on probability measures," *Journal of Machine Learning Research*, vol. 11, no. 4, pp. 1517–1561, 2010.
- [20] A. Gretton, K. M. Borgwardt, M. J. Rasch, B. Schölkopf, and A. Smola, "A kernel two-sample test," *Journal of Machine Learning Research*, vol. 13, no. 3, pp. 723–773, 2012.
- [21] Y. Mroueh, T. Sercu, and V. Goel, "Mcgan: Mean and covariance feature matching gan," *International conference on Machine Learning*, 2017.
- [22] C.-L. Li, W.-C. Chang, Y. Cheng, Y. Yang, and B. Póczos, "Mmd gan: Towards deeper understanding of moment matching network," *Advances in Neural Information Processing Systems*, 2017.
- [23] K. Saenko, B. Kulis, M. Fritz, and T. Darrell, "Adapting visual category models to new domains," in *European Conference on Computer Vision*, pp. 213–226, Springer, 2010.
- [24] L. Bruzzone and M. Marconcini, "Domain adaptation problems: A dasvm classification technique and a circular validation strategy," *IEEE Transactions on Pattern Analysis and Machine Intelligence*, vol. 32, no. 5, pp. 770–787, 2010.
- [25] M. Baktashmotlagh, M. T. Harandi, B. C. Lovell, and M. Salzmann, "Unsupervised domain adaptation by domain invariant projection," in *IEEE International Conference on Computer Vision*, pp. 769–776, 2013.
- [26] C. Cortes and M. Mohri, "Domain adaptation and sample bias correction theory and algorithm for regression," *Theoretical Computer Science*, vol. 519, pp. 103–126, 2014.
- [27] W. Li and X. Wang, "Locally aligned feature transforms across views," in *IEEE Conference on Computer Vision and Pattern Recognition*, pp. 3594–3601, 2013.
- [28] M. Long, H. Zhu, J. Wang, and M. I. Jordan, "Unsupervised domain adaptation with residual transfer networks," in *Advances in Neural Information Processing Systems*, pp. 136–144, 2016.
- [29] M. Long, J. Wang, and M. I. Jordan, "Deep transfer learning with joint adaptation networks," *International Conference on Machine Learning*, 2017.
- [30] Y. Li, N. Wang, J. Shi, J. Liu, and X. Hou, "Revisiting batch normalization for practical domain adaptation," *International Conference on Learning Representations Workshop*, 2017.
- [31] B. Sun, J. Feng, and K. Saenko, "Return of frustratingly easy domain adaptation," in *AAAI Conference on Artificial Intelligence*, 2016.
- [32] M. Arjovsky and L. Bottou, "Towards principled methods for training generative adversarial networks," *International Conference on Learning Representations*, 2017.
- [33] A. Gretton, K. M. Borgwardt, M. Rasch, B. Schölkopf, and A. J. Smola, "A kernel method for the two-sample-problem," in *Advances in Neural Information Processing Systems*, pp. 513–520, 2006.
- [34] E. Tzeng, J. Hoffman, N. Zhang, K. Saenko, and T. Darrell, "Deep domain confusion: Maximizing for domain invariance," *arXiv preprint arXiv:1412.3474*, 2014.
- [35] G. Csúrká, B. Chidlowskii, S. Clinchant, and S. Michel, "Unsupervised domain adaptation with regularized domain instance denoising," in *Computer Vision—ECCV 2016 Workshops*, pp. 458–466, Springer, 2016.
- [36] K. Fukumizu, A. Gretton, G. R. Lanckriet, B. Schölkopf, and B. K. Sriperumbudur, "Kernel choice and classifiability for rkhs embeddings of probability distributions," in *Advances in Neural Information Processing Systems*, pp. 1750–1758, 2009.
- [37] K. Bousmalis, G. Trigeorgis, N. Silberman, D. Krishnan, and D. Erhan, "Domain separation networks," in *Advances in Neural Information Processing Systems*, pp. 343–351, 2016.
- [38] W. Zellinger, T. Grubinger, E. Lughofer, T. Natschlager, and S. Saminger-Platz, "Central moment discrepancy (cmd) for domain-invariant representation learning," *International Conference on Learning Representations*, 2017.
- [39] A. Krizhevsky, I. Sutskever, and G. E. Hinton, "Imagenet classification with deep convolutional neural networks," in *Advances in Neural Information Processing Systems*, pp. 1097–1105, 2012.
- [40] M. Sugiyama, S. Nakajima, H. Kashima, P. V. Buenau, and M. Kawanabe, "Direct importance estimation with model selection and its application to covariate shift adaptation," in *Advances in Neural Information Processing Systems*, pp. 1433–1440, 2008.
- [41] J. Huang, A. Gretton, K. M. Borgwardt, B. Schölkopf, and A. J. Smola, "Correcting sample selection bias by unlabeled data," in *Advances in Neural Information Processing Systems*, pp. 601–608, 2007.
- [42] V. M. Zolotarev, "Probability metrics," *Teoriya Veroyatnostei i ee Primeneniya*, vol. 28, no. 2, pp. 264–287, 1983.
- [43] R. M. Dudley, *Real analysis and probability*, vol. 74. Cambridge University Press, 2002.
- [44] N. I. Achieser, *Theory of approximation*. Courier Corporation, 2013.
- [45] C. Clenshaw, "A note on the summation of chebyshev series," *Mathematics of Computation*, vol. 9, no. 51, pp. 118–120, 1955.
- [46] M.-K. Hu, "Visual pattern recognition by moment invariants," *IRE Transactions on Information Theory*, vol. 8, no. 2, pp. 179–187, 1962.
- [47] Y. Rui, T. S. Huang, and S.-F. Chang, "Image retrieval: Current techniques, promising directions, and open issues," *Journal of Visual Communication and Image Representation*, vol. 10, no. 1, pp. 39–62, 1999.
- [48] N. Aronszajn, "Theory of reproducing kernels," *Transactions of the American Mathematical Society*, vol. 68, no. 3, pp. 337–404, 1950.
- [49] S. T. Rachev, L. Klebanov, S. V. Stoyanov, and F. Fabozzi, *The methods of distances in the theory of probability and statistics*. Springer Science & Business Media, 2013.
- [50] C. Kleiber and J. Stoyanov, "Multivariate distributions and the moment problem," *Journal of Multivariate Analysis*, vol. 113, pp. 7–18, 2013.
- [51] J. Duchi, E. Hazan, and Y. Singer, "Adaptive subgradient methods for online learning and stochastic optimization," *Journal of Machine Learning Research*, vol. 12, no. Jul, pp. 2121–2159, 2011.
- [52] M. D. Zeiler, "Adadelta: an adaptive learning rate method," *arXiv preprint arXiv:1212.5701*, 2012.
- [53] C. Louizos, K. Swersky, Y. Li, M. Welling, and R. Zemel, "The variational fair auto encoder," *International Conference on Learning Representations*, 2016.
- [54] J. Fan and J. S. Marron, "Fast implementations of nonparametric curve estimators," *Journal of Computational and Graphical Statistics*, vol. 3, no. 1, pp. 35–56, 1994.
- [55] E. Zhong, W. Fan, Q. Yang, O. Verscheure, and J. Ren, "Cross validation framework to choose amongst models and datasets for transfer learning," in *Joint European Conference on Machine Learning and Knowledge Discovery in Databases*, pp. 547–562, Springer, 2010.
- [56] F. Chollet, "Keras: Deep learning library for theano and tensorflow," 2015.
- [57] B. K. Sriperumbudur, K. Fukumizu, A. Gretton, G. R. Lanckriet, and B. Schölkopf, "Kernel choice and classifiability for rkhs embeddings of probability distributions," in *Advances in Neural Information Processing Systems*, pp. 1750–1758, 2009.
- [58] A. Gretton, D. Sejdinovic, H. Strathmann, S. Balakrishnan, M. Pontil, K. Fukumizu, and B. K. Sriperumbudur, "Optimal kernel choice for large-scale two-sample tests," in *Advances in Neural Information Processing Systems*, pp. 1205–1213, 2012.
- [59] C.-W. Hsu, C.-C. Chang, and C.-J. Lin, "A practical guide to support vector classification," 2003.
- [60] A. Madansky, "Bounds on the expectation of a convex function of a multivariate random variable," *The Annals of Mathematical Statistics*, vol. 30, no. 3, pp. 743–746, 1959.
- [61] M. Egozcue, L. F. García, W. K. Wong, and R. Zitikis, "The smallest upper bound for the pth absolute central moment of a class of random variables," *The Mathematical Scientist*, 2012.